SAND2011-2009C

ILASS Americas, 23rd Annual Conference on Liquid Atomization and Spray Systems, Ventura, CA, May 2011

Chemiluminescence and Fuel PLIF Imaging of Reactivity Controlled Compression Ignition (RCCI) Combustion

S. L. Kokjohn* and R. D. Reitz
Department of Mechanical Engineering
University of Wisconsin-Madison
Madison, WI 53706 USA

M. P. B. Musculus
Combustion Research Facility
Sandia National Laboratory
Livermore, CA 94550 USA

Abstract

In recent years, many premixed compression ignition (PCI) strategies have demonstrated high-efficiency and low pollutant emissions. However, PCI operation is generally confined to low engine loads due to the rapid energy release resulting from volumetric combustion. Furthermore, the injection event is typically decoupled from the ignition event, which presents challenges for controlling the combustion phasing. One PCI strategy, dual-fuel reactivity controlled compression ignition (RCCI), has been developed to address the issues of combustion phasing and rate-of-heat release control. The RCCI concept uses in-cylinder blending of two fuels with different auto-ignition characteristics to achieve controlled high-efficiency clean-combustion.

Recent experiments conducted on an all metal heavy-duty diesel research engine have demonstrated that dual-fuel RCCI operation can offer high-efficiency with low engine-out pollutant emissions. However, the mechanisms controlling the energy release in RCCI combustion are not well understood. Accordingly, the present study explores the RCCI concept using an optically accessible, heavy-duty, single-cylinder research engine. The research engine is equipped with two fuel systems to allow for in-cylinder fuel blending. Iso-octane is delivered using a low-pressure (100 bar) gasoline direct injector (GDI) and n-heptane is delivered through a higher pressure (600 bar) common-rail (CR) diesel direct-injector. The first part of this study uses a CMOS high-speed camera to image the ensuing combustion luminosity, composed primarily of chemiluminescence. The chemiluminescence imaging shows that at the operating condition studied in the present work (4 bar IMEP and 1200 rev/min), ignition typically occurs first in the squish region. Subsequent combustion propagates inward towards the centrally mounted common-rail injector. The second part of this study investigates the charge preparation of the RCCI strategy using planar laser induced fluorescence (PLIF) of a fuel tracer under non-reacting conditions to image the fuel distribution prior to ignition. Ensemble-averaged fuel concentration measurements show that the fuel reactivity generally increases with increasing axial position from the common-rail injector. Thus, it appears that the ignition location is determined by a region of high-fuel reactivity in the outer region of the combustion chamber. The observed progression of the reaction zone from the outer-to-inner region of the combustion chamber is at least partially controlled by the gradient in fuel reactivity.

*Corresponding author

Introduction

Highly premixed compression ignition (PCI) strategies (e.g., homogenous charge compression ignition (HCCI)) offer attractive emissions and performance characteristics (i.e., high efficiency and low NOx and soot emissions) **[1-3]**. However, these operating strategies are generally confined to low engine loads due to difficulties controlling the heat-release rate and lack of an adequate combustion phasing control mechanism. Recently, Sjöberg et al. **[4]** proposed that partial fuel stratification may be a promising method to control the heat-release rate for HCCI engines. Additionally, Dec et al. **[5, 6]** have suggested that harnessing natural thermal stratification may be a key to controlling HCCI heat-release rates and increasing the HCCI operating range. Both thermal and equivalence ratio stratification introduce non-uniformities in the auto-ignition characteristics of the charge. These non-uniformities result in a staged ignition event, which tends to reduce the peak heat-release rate.

Kokjohn et al. **[1]** proposed blending two fuels with different auto-ignition characteristics inside the combustion chamber to artificially generate non-uniformities in the auto-ignition characteristics of the charge. Using metal engine experiments, Hanson et al. **[2]** and Kokjohn et al. **[7]** showed that stratifying the fuel reactivity via in-cylinder fuel blending improves the control over the heat-release rate and allows an extension of the PCI combustion regime to higher engine loads. Consequently, they termed this alternative combustion mode "reactivity-controlled compression-ignition," or RCCI. Further, the metal engine experiments have shown that RCCI combustion can achieve gross indicated efficiencies over 50 percent for a wide range of operating conditions while meeting current, heavy-duty, on-highway NOx and soot emissions limits in-cylinder. The high-efficiency is primarily due to reductions in heat transfer losses by avoiding high temperature regions **[8]**. Although they are useful to understand emissions and performance tradeoffs, details of the dominant in-cylinder processes controlling RCCI combustion cannot be observed in metal engine experiments.

In an attempt to improve the fundamental understanding of RCCI combustion, Splitter et al. **[9]** used in-cylinder Fourier-transform infrared (FTIR) spectroscopy to investigate the evolution of the RCCI combustion process. FTIR spectra were acquired at two locations, to provide a degree of spatial resolution, and were indexed to engine crank-angle to give cycle-averaged, crank-angle-resolved in-cylinder spectroscopy. Their results suggested that the RCCI combustion process proceeded at different rates in different locations of the cylinder. However, their measurements were restricted by the limited optical access of their engine. Additionally, several studies have used detailed CFD modeling (e.g., Kokjohn et al. **[8]**) with reduced kinetics mechanisms to investigate RCCI combustion. The CFD modeling predicted that non-uniformities in the auto-ignition characteristics of the charge, generated by in-cylinder fuel blending, control the heat-release rate. In the present study, RCCI combustion is investigated in a heavy-duty, single cylinder, optically accessible research engine using a combination of high-speed chemiluminescence imaging and fuel-tracer planar laser-induced fluorescence (PLIF).

Engine Specifications and Operating Conditions

A single-cylinder, direct-injection (DI), 4-stroke diesel engine based on a Cummins N14 production engine was used for this investigation. A schematic of the engine and optical setups are shown in Figure 1 and specifications are given in Table 1. The research engine is typical of a heavy-duty diesel engine with a 13.97-cm bore and 15.24-cm stroke giving a displacement of 2.34 L per cylinder. The intake port geometry of the production engine, which has a steady-state (i.e., measured on a flow-bench) swirl ratio of 0.5 [10], is preserved in the research engine.

Table 1. Engine Specifications

Engine base type	Cummins N-14, DI diesel
Number of cylinders	1
Cycle	4-stroke
Number of intake valves	2
Number of exhaust valves	1*
Combustion chamber	Quiescent, direct injection
Swirl Ratio	0.5 (approximate)
Bore	13.97 cm [5.5 in]
Stroke	15.24 cm [6.0 in]
Bowl width	9.78 cm [3.58 in]
Displacement	2.34 liters [142 in^3]
Connecting rod length	30.48 cm [12.0 in]
Piston pin offset	None
Geometric compression ratio	10.75:1

*In this optically accessible diesel engine, one of the two exhaust valves of the production cylinder head has been replaced by a window and periscope

To allow optical access, the engine is equipped with an extended piston and the stock metal piston bowl has been replaced with a flat fused silica piston crown window. Further, one of the two exhaust valves has been replaced with a window, and a periscope mirror in the rocker box gives a view of the squish region (i.e., the region above the piston bowl-rim). Four windows are also located around the upper portion of the cylinder wall to allow cross-optical access for laser based diagnostics.

Fuel Injection Systems

RCCI combustion is achieved by using in-cylinder blending of two fuels with different auto-ignition cha-

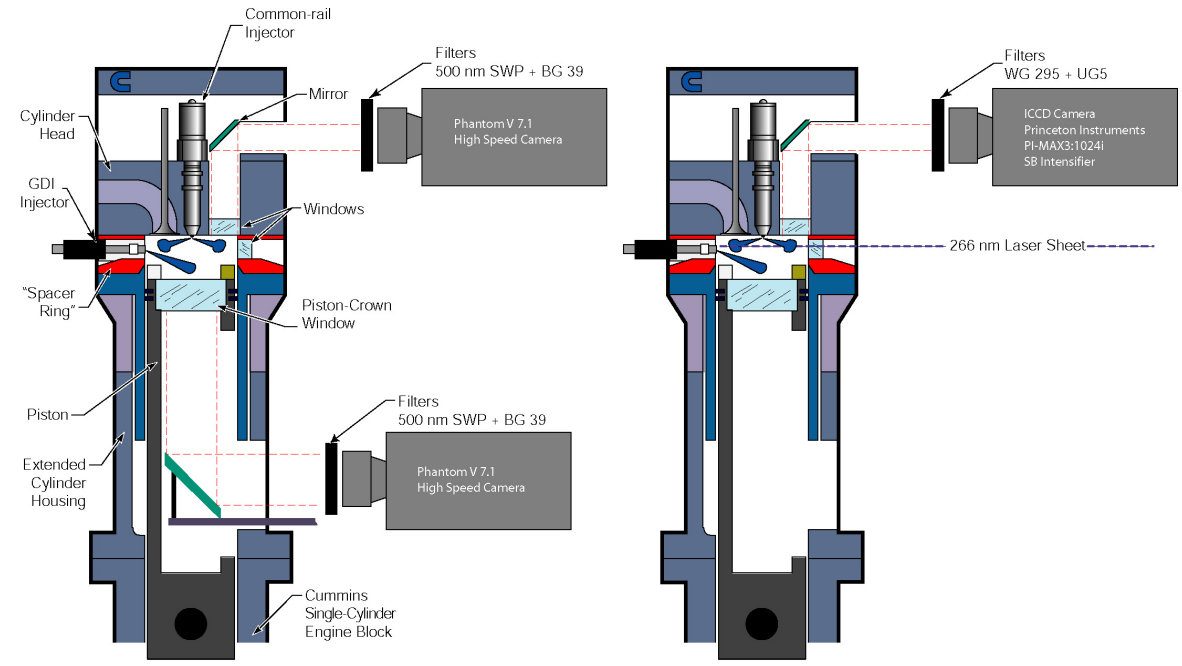

Figure 1. Schematic of the optically accessible research engine. (a) shows the camera setup for the high-speed chemiluminescence imaging study and (b) shows the camera and laser sheet setup for the fuel tracer PLIF study.

racteristics, such as gasoline and diesel fuels. Multi-component gasoline and diesel fuels contain molecules that fluorescence when illuminated by ultraviolet light, which would interfere with the toluene fuel-tracer fluorescence diagnostic (described later). To facilitate the fuel-tracer measurements, purified gasoline primary reference fuel (PRF) components (i.e., n-heptane and iso-octane) were used because they display insignificant fluorescence interference. A charge of high-performance liquid chromatography (HPLC) grade iso-octane was created using a gasoline direct injection (GDI) system. The GDI injector is mounted in a metal blank in place of one of the optical access windows formerly located in the cylinder liner (see Figure 1). The specifications of the GDI injector are provided in Table 2. The GDI has a 7-hole, asymmetric tip, with all seven holes located on one hemisphere of the injector. This hole layout allowed the fuel to avoid impingement on the cylinder head when mounted in the cylinder wall window (i.e., perpendicular to the axis of the piston). The other fuel, HPLC-grade n-heptane, was delivered through a Cummins XPI high-pressure, electronically-controlled, common-rail fuel injector with specifications given in Table 3. The injector is capable of multiple injections at up to 2000 bar injection pressure. For the present study, an 8-hole mini-sac tip was installed. In this tip, each hole has a nominal orifice diameter of 140 microns with no hydrogrounding (i.e., the edges are sharp). The nozzle has an included angle of 152° (14° downward from the fire deck, i.e., the bottom surface of the cylinder head exposed to the combustion chamber). Finally, to minimize thermal loading, the engine was only fired 1 out of 10 cycles.

Table 2. Gasoline direct injection (GDI) injector specifications.

Injector type	GDI
Fuel	HPLC grade iso-octane
Number of holes	7, asymmetric
Supply pressure	100 bar
Nominal orifice diameter	150 micron

Table 3. XPI common-rail fuel injector specs.

Injector type	common-rail, solenoid actuated
Fuel	HPLC-grade n-heptane
Cup (tip) type	mini-sac
Number of holes	8, equally spaced
Included angle	152°
Rail pressure	600 bar
Orifice treatment	none (square-edged)
Nominal orifice diameter	140 micron

Operating condition

The engine operating conditions for the chemiluminescence imaging study are shown in Table 4. The engine was operated at a speed of 1200 rev/min and a gross indicated mean effective pressure (IMEP) of

4.2 bar. This light-load condition was chosen to avoid damaging the large piston crown window. Under the operating conditions of the current study, the peak heat-release rate for the 4.2 bar load is well below the allowable threshold for the optical engine. However, some conditions in a parametric variation of injection timing in part of a larger study (not shown here) have much higher peak heat-release rates, so the engine load was restricted to 4.2 bar IMEP.

Table 4. Engine operating condition for the chemiluminescence imaging study and reference operating condition for the toluene fuel tracer fluorescence study.

Engine speed	1200 rpm
Gross IMEP	4.2 bar
Intake temperature	90°C
Intake pressure	1.1 bar abs.
Inlet oxygen concentration	21 vol. %
GDI injection pressure	100 bar
CR injection pressure	600 bar
GDI SOI (command)	-240° ATDC
CR SOI 1 (actual)	-57° ATDC
CR SOI 2 (actual)	-37° ATDC
Actual GDI DOI	36° CA
Actual CR DOI1	7° CA
Actual CR DOI2	4° CA
Total injected fuel mass	62 mg
iso-octane mass (GDI)	66%
n-heptane mass (CR)	34%
Quantity of injected fuel in CR Inj.1	12.6
Quantity of injected fuel in CR Inj. 2	8.4
Premixed (iso-octane) equivalence ratio	0.27
Overall equivalence ratio	0.42
Nom. motored TDC density	11.1 kg/m^3
Nom. motored TDC temperature	835 K

With the intent of creating a well-mixed charge of iso-octane, 41 mg of iso-octane was delivered through the GDI injector at -240° ATDC (during the intake stroke) at an injection pressure of 100 bar. The n-heptane was delivered through the common-rail injector at a pressure of 600 bar using a split-injection with a first pulse beginning at -57° ATDC and a second pulse beginning at -37° ATDC. The total injected mass of n-heptane was 21 mg and approximately 60% of the n-heptane was delivered in the first injection (i.e., at -57° ATDC). The engine was operated without dilution (i.e., the inlet oxygen concentration was 21% by volume) and the intake pressure was set to slightly above atmospheric at 1.1 bar absolute. The intake temperature was set to 90° C to give a density at TDC of 11.1 kg/m^3.

The toluene fuel-tracer fluorescence study was conducted at the same thermodynamic conditions as the chemiluminescence imaging study; however, to avoid complications from oxygen quenching of the toluene fluorescence, the intake was supplied with 100% nitrogen. Further, HPLC n-heptane doped with 1% toluene was used in both the GDI and common-rail fuel systems for quantitative fuel distribution measurements. We chose to use the same toluene-doped n-heptane in both fuel systems (non-combusting conditions) to avoid uncertainties in the toluene fluorescence yield in different solvents.

Chemiluminescence Imaging

Crank-angle resolved high temperature chemiluminescence was recorded with a Phantom 7.1 complementary metal oxide semiconductor (CMOS) high-speed camera (HSC) using a 50 mm glass Nikkor lens with the aperture fully open (f/1.2). Because a glass lens was used, chemiluminescence in the ultra-violet (UV) range is not recorded (i.e., OH* does not contribute to the images presented). Furthermore, a combination of a 500 nm short-wave pass (SWP) filter and a BG39 colored glass filter were used to reject long-wavelength (green through IR) soot luminosity. However, at the operating conditions of the present study, the pre-combustion mixing time is sufficiently long that soot levels are expected to be very low. Indeed, operation at a similar condition in an all metal engine **[11]** showed negligible exhaust soot. With the imaging setup used in this study, the recorded luminosity is likely chemiluminescence from CH_2O*, HCO*, CH*, and CO_2* and broadband emission from the CO continuum **[5, 12]**. The HSC images were acquired with a resolution of 512 x 512 pixels and the exposure time for each frame was 125 μs.

Fuel-Tracer Fluorescence Imaging

Quantitative fuel-vapor concentrations were measured using toluene fuel-tracer fluorescence. As previously discussed, the n-heptane used for the fuel-tracer fluorescence imaging study was doped with toluene at a concentration of 1% by volume. Previous work (e.g., Genzale et al. **[13]**) showed that this toluene concentration provided a good balance between signal strength and undue attenuation of the laser light. The toluene fluorescence was excited by the 266 nm output of a frequency-quadrupled Nd:YAG laser. The laser beam was formed into a thin sheet (less than 1 mm thick) using a combination of a negative cylindrical lens (f = -50 mm) and positive plano-spherical lens (f = 500 mm). The tails on either end of the sheet were clipped to improve the uniformity of the laser sheet intensity distribution. After being clipped, the sheet passing through the window was approximately 31 mm wide and the recorded laser energy was 26 mJ per pulse. All of the images presented in this study were acquired with the sheet positioned 10 mm below the firedeck (i.e., the flat bottom surface of the cylinder-head).

A blue-optimized intensified CCD camera (Princeton Instruments PI-MAX3:1024i) with a 55 mm f/3.5

UV lens with the aperture fully open imaged the resulting florescence viewing downward through the cylinder head window (see Figure 1b). A WG295 long-wave pass (LWP) filter helped to isolate the toluene fluorescence (265-330 nm **[14]**) from scattered laser light. Additionally, a UG5 UV-bandpass filter (passband in the range of 220 to 400 nm) blocked red-shifted fluorescence from motor oil and other sources **[14]**.

To perform quantitative fuel-vapor concentration measurements, calibration of the toluene fluorescence with a known fuel/tracer concentration is required. In this work calibration images at a known fuel/tracer concentration were obtained by injecting toluene-doped n-heptane, using the common-rail injector, near TDC of the intake stroke. In similar studies (e.g., Musculus et al. **[15]**) early-cycle injections of low boiling-range fuels have been shown to yield acceptably homogenous mixtures. Indeed, the calibration images of this study appear reasonably uniform. Although the calibration images appear nearly homogeneous, it is possible that non-uniformities exist outside of the camera field of view. These non-uniformities, if present, introduce uncertainty into the vapor fuel concentration measurements of this study, though it is not possible to quantify this level of uncertainty in the present work. Further, with the early cycle injection used in this study, some liquid may impinge on the combustion chamber surfaces; however, the intake temperature and coolant temperature were set to near the atmospheric boiling point of n-heptane. Thus, it is likely that any liquid impinging on a combustion chamber surface would rapidly vaporize. However, it should be noted that if liquid fuel does remain at the imaging time, the fuel vapor concentration measurements would be biased towards higher fuel concentrations.

Fuel-vapor concentration measurements were performed for separate injections from both the common-rail and GDI fuel systems. At each crank angle of interest, images were acquired in sets of four. The first image provided a flat-field calibration at a known toluene/fuel concentration as previously discussed. The second and third images recorded fluorescence from the fuel injected through the GDI only and common-rail injector only, respectively. The fourth image had no fuel injection and recorded background fluorescence interference – likely due to residual oil excited by scattered laser light **[14, 15]**. This four-image sequence was repeated 40 times at each crank angle of interest. The raw PLIF images were then corrected for temperature and converted to fuel concentrations as described by Musculus et al. **[15]**. Of interest to this study are the relative concentrations of fuel from the GDI and common-rail fuel streams. Thus, a PRF number is defined as

$$PRF = 100\frac{m_{GDI}/\rho_{\text{iso-octane}}}{m_{GDI}/\rho_{\text{iso-octane}} + m_{CR}/\rho_{\text{n-heptane}}} \quad (1)$$

where the m_{GDI} is the measured vapor-fuel mass from the GDI images corrected for the difference in molecular weight of iso-octane and n-heptane, m_{CR} is the mass of n-heptane measured from the common-rail (CR) injection images, and $\rho_{\text{iso-octane}}$ and $\rho_{\text{n-heptane}}$ are the densities of liquid iso-octane and n-heptane, respectively. This definition of PRF number is equivalent to a volume percent of iso-octane in the fuel blend for each pixel.

Results and Discussion

Cylinder Pressure and Heat Release Rate

Cylinder pressure was measured with a piezoelectric transducer at ¼° crank angle increments and the measurements were set to match (pegged) the intake pressure near bottom dead center (BDC). The apparent heat release rate (AHRR) was calculated from the measured pressure data using the standard first-law analysis (e.g., Heywood **[16]**) with constant gas properties. Prior to calculating the AHRR, the cylinder pressure data were smoothed using a Fourier series low-pass filter with a Gaussian roll-off function having a transmission of 100% from 0 to 800 Hz and dropping to 1% at 3360 Hz. At the operating condition investigated in the present work, the energy release occurs rather slowly; thus, the selected filtering scheme removes acoustic ringing with virtually no effect on the shape of the AHRR curve.

Figure 2 shows the measured cylinder pressure, common-rail fuel injector command signal, and appar-

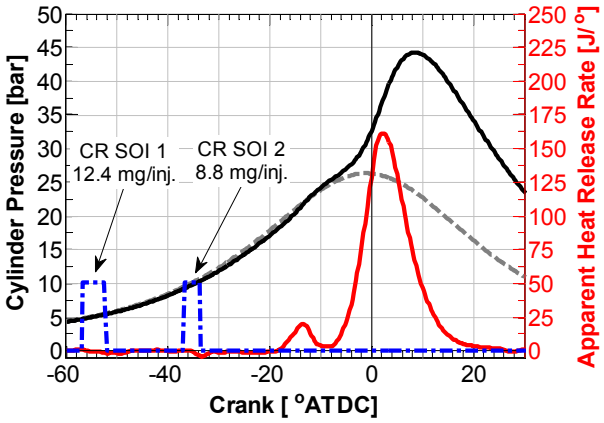

Figure 2. Measured cylinder pressure (fired and motored), common-rail injector logic signal, and apparent heat-release rate. The GDI injection of iso-octane has an SOI timing of -240° ATDC (not shown).

ent heat release rate. The first common rail injection of n-heptane begins at -57° ATDC. Near -40° ATDC the evaporative cooling and an increase in the heat capacity of the charge resulting from the GDI and first common-rail injections causes the cylinder pressure recorded on the fired cycle to fall slightly below that of the motored trace. At -37° ATDC the second common rail injection begins and the associated evaporative cooling causes the pressure to further drop below the motored trace. Around -19° ATDC, low-temperature reactions push the apparent heat release rate above zero. The energy release from these low-temperature reactions reaches a peak near -13° ATDC and by -11° ATDC enough energy has been released from low-temperature reactions to raise the cylinder pressure above the motored pressure. Because iso-octane is a single stage fuel[1] (i.e., it generally does not exhibit low temperature heat release) it is expected that the observed low-temperature heat release is primarily the result of n-heptane decomposition. Indeed, Puduppakkam et al. **[17]** used CFD modeling coupled with a detailed chemical kinetic mechanism to study RCCI combustion and found that the low temperature heat release was primarily due to n-heptane decomposition. After peaking, the energy release decreases to near zero at -10° ATDC and the heat release curve remains relatively flat until -7° ATDC. The high-temperature heat-release begins near -7° ATDC and peaks near 2° ATDC. The relatively symmetric shape of the high-temperature heat release curve suggests that no mixing controlled combustion is present, consistent with the long ignition dwell. However, in comparison to perfectly mixed conditions, the energy release occurs rather slowly (if the charge were perfectly premixed, chemical kinetics calculations show that the charge would ignite nearly uniformly (volumetrically) and the combustion event would be completed within a few crank angle degrees).

Combustion Chemiluminescence Imaging

Figure 3 shows the field of view (FOV) for each camera setup used for the combustion chemiluminescence imaging study. The image on the left-hand side shows the recorded luminosity with the HSC viewing upward through the flat piston crown window, while the image on the right-hand side shows the combustion luminosity recorded with the HSC viewing downward through the cylinder head window. Although each pair of bottom-view and top-view images were acquired at the same crank angle, they are from different cycles (only one camera), so they are not simultaneous. The time in crank angle degrees after top dead center is shown in the upper left-hand corner of each image. The solid gray line on the piston crown window images shows the inner edge of the piston bowl rim, which also bounds the field of view (FOV) of the images acquired through the piston crown window. The FOV of the cylinder head window images is shown by the white dashed line on both images. Notice that approximately 1/3 of the FOV of the cylinder head window images overlaps with the FOV of the piston crown window. The images acquired through the cylinder-head window view downward onto the top of the piston bowl rim, as indicated by the solid gray lines.

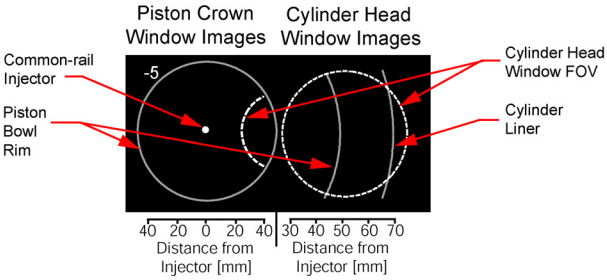

Figure 3. Camera field of view for both imaging locations. Note that the cylinder head window images are enlarged by a scale factor of 1.7 to more clearly show the ignition process.

Selected high-temperature combustion chemiluminescence images are shown in Figure 4. The presented images are selected from a single cycle that had an AHRR most similar to the ensemble-average AHRR in Figure 2. The appearance of chemiluminescence in the downstream region of the jet between -5° and -7° ATDC coincides with the transition to second-stage combustion (i.e., high-temperature ignition). Small ignition pockets are initially observed in two locations, inside the edge of the piston bowl rim, and in the squish region (i.e., above the piston bowl-rim). These ignition zones grow for several crank angles while more ignition pockets continue to appear. The separate ignition pockets then merge into larger, more coherent reaction zones. By -1° ATDC, the squish window image is nearly filled with combustion luminosity[2]. The remainder of the images show that the reaction zones move steadily back upstream towards the centrally mounted common-rail injector. Notice that careful inspection of the reaction zones shows that small auto-ignition pockets appear ahead of the main reaction zone. This suggests that the mechanism for reaction

[1]Dec et al. **[19]** have shown that under some conditions (e.g., low engine speed), iso-octane does show low-temperature heat release; however, the present study operates at conditions where iso-octane is expected to behave as a single stage fuel.

[2]Note that the presented images are integrated in the line-of-sight; therefore, it is not possible to determine the level of combustion luminosity into the page (i.e., it is possible that the observed luminosity is occurring at different distances orthogonal to the firedeck).

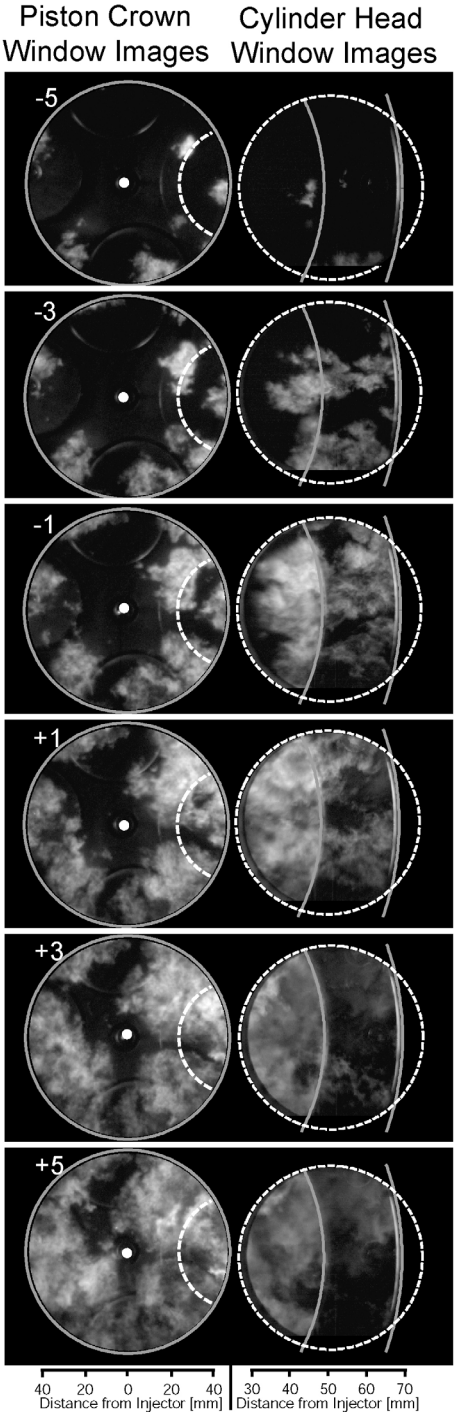

Figure 4. High-speed camera image sequence of RCCI combustion. The images on the left-hand side were acquired with the HSC viewing upward through the flat piston crown window, while the images on the right-hand side were acquired looking downward through the cylinder head window. Note that two sets of images were not acquired simultaneously. See Figure 3 for a description of the image layout.

zone movement is sequential auto-ignition; however, more work is required to definitively determine the dominant mechanism of reaction zone growth.

As an alternative visualization of the reaction zone progression, ignition maps **[18]** were created from the representative HSC image sequence. To generate the ignition maps, the images were first normalized by a reference image prior to combustion. In this study the image at -10° ATDC was selected as the pre-combustion image. The ignition crank angle for each pixel was then defined as the time when the luminosity increased by 20 percent over the pre-combustion image. While the level of the threshold value is somewhat arbitrary, the resulting ignition map is not strongly influenced by the threshold level. Further note that the camera setup used in this study was not sensitive enough to capture the weak luminosity from low-temperature reactions; therefore, it was not necessary to distinguish between first- and second-stage combustion luminosity. The ignition map shown in Figure 5 clearly shows a progression of the high-temperature reaction zone from the downstream portion of the jet to the cylinder centerline.

Spray and Charge Preparation Imaging

The chemiluminescence imaging study showed that ignition generally occurred near the edge of the piston bowl rim and in the squish region. Once ignition occurred, the reaction zone then moved upstream towards the centrally mounted common-rail injector. To understand the preferential downstream ignition and upstream reaction-zone progression, the toluene fluorescence diagnostic was used to measure the fuel distribution prior to ignition. Additionally, liquid fuel sprays were illuminated with two high-power light emitting diodes (LED) for imaging using the high speed camera.

Figure 6 shows liquid-fuel images and the ensemble-averaged PRF maps at several times during the common-rail injection event. The liquid fuel images, shown with a black background, are from a representative single cycle and were acquired with the HSC viewing upward through the piston crown window, as discussed in the chemiluminescence imaging section. Recall that the FOV of the images acquired viewing upward through the piston crown window is bounded by the piston bowl rim, indicated by the inner (leftmost) solid gray line drawn on the HSC images. Additionally, to facilitate comparisons between the PRF maps and the liquid fuel images, the outer solid gray line drawn on the HSC images shows the location of the cylinder liner. The PRF maps are ensemble averaged over 40 cycles viewing downward through the cylinder-head window. The solid gray line on the left-hand side of each PRF map shows the edge of the cylinder-head window FOV. The FOV of the cylinder head window is also indicated on the HSC images by the dashed

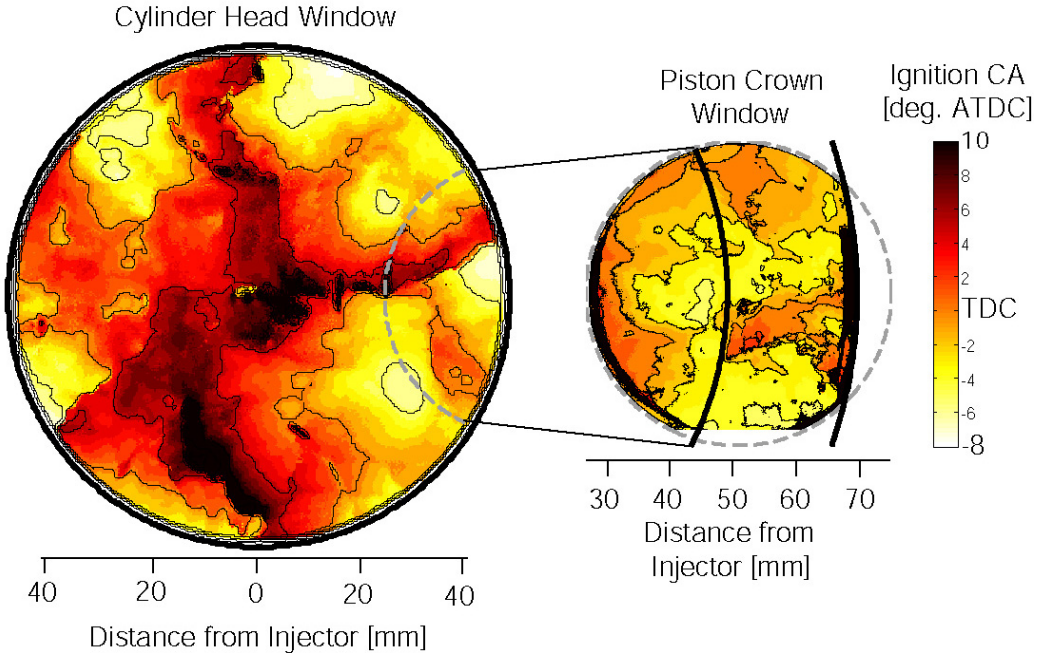

Figure 5. Ignition map for split-injection dual-fuel RCCI operation. Light regions show the earliest ignition locations and dark regions show the latest ignition locations.

white line. The middle gray line on the PRF maps shows the location of the piston bowl rim and the gray line on the right-hand side of each image shows the location of the cylinder liner. The laser sheet enters from the right-hand side of each image and the approximate area of the PRF maps is indicated by the green lines on the HSC images. Notice that the scale of the PRF map is increased compared to the HSC images to highlight the key features.

The fuel enters the field of view of the cylinder head window images around -53° ATDC. Note that at this time it is likely that some liquid fuel remains, evident from the HSC images; thus, the fuel concentration measurements at this crank angle are likely biased by fluorescence and scattering from liquid fuel, and should be considered as upper bounds. Shortly later, at -50° ATDC, the HSC images show that the injection is nearly complete and very little liquid fuel is present in the images. At this time the fuel-tracer PLIF images show that the vapor fuel has penetrated nearly to the cylinder liner[3].

[3] The solid gray box in the -50° ATDC indicates a region where strong fluorescence from lubricating oil interferes with the fuel concentration measurements in that image only. The in-cylinder surfaces were thoroughly cleaned of oil prior to imaging runs to mitigate any such interference, but unfortunately, in the -50° ATDC run, some oil remained in the corner of the image.

By -45° ATDC the vapor fuel from the first injection has penetrated to the liner and is beginning to spread along the cylinder wall. Although the fuel injection is over, momentum causes the vapor fuel to continue to penetrate, entraining ambient gas (air and iso-octane), and the PRF number in the upstream portion begins to rapidly decrease. Post injection mixing continues and shortly before the fuel vapor from the second common-rail injection enters the FOV (i.e., the images at -40° and -35° ATDC), the minimum PRF number in the plane of the laser sheet is 50 to 60.

At -30° ATDC, the fuel jet from the second injection enters the FOV and mixes with the fuel from the GDI and first common rail injection. Notice that due to slower penetration at the higher ambient densities for the second injection, by the time vapor fuel enters the FOV of the cylinder head window, the fuel injection process is complete. Similar to the first injection, the vapor-fuel jet continues to penetrate after the end of injection; however, now the jet is entraining not only nitrogen (air in the case of combusting conditions) and iso-octane, but also n-heptane from the first injection. Because the n-heptane concentration tends to increase away from the nozzle (i.e., towards the liner), the PRF number of the entrained fuel tends to decrease as the jet moves downstream. By -25° ATDC the ensemble-averaged PRF number in head of the jet from the second common rail injection has increased to around 50 (i.e., a 50 – 50 blend of iso-octane and n-heptane). Notice that outside of the region influenced by the

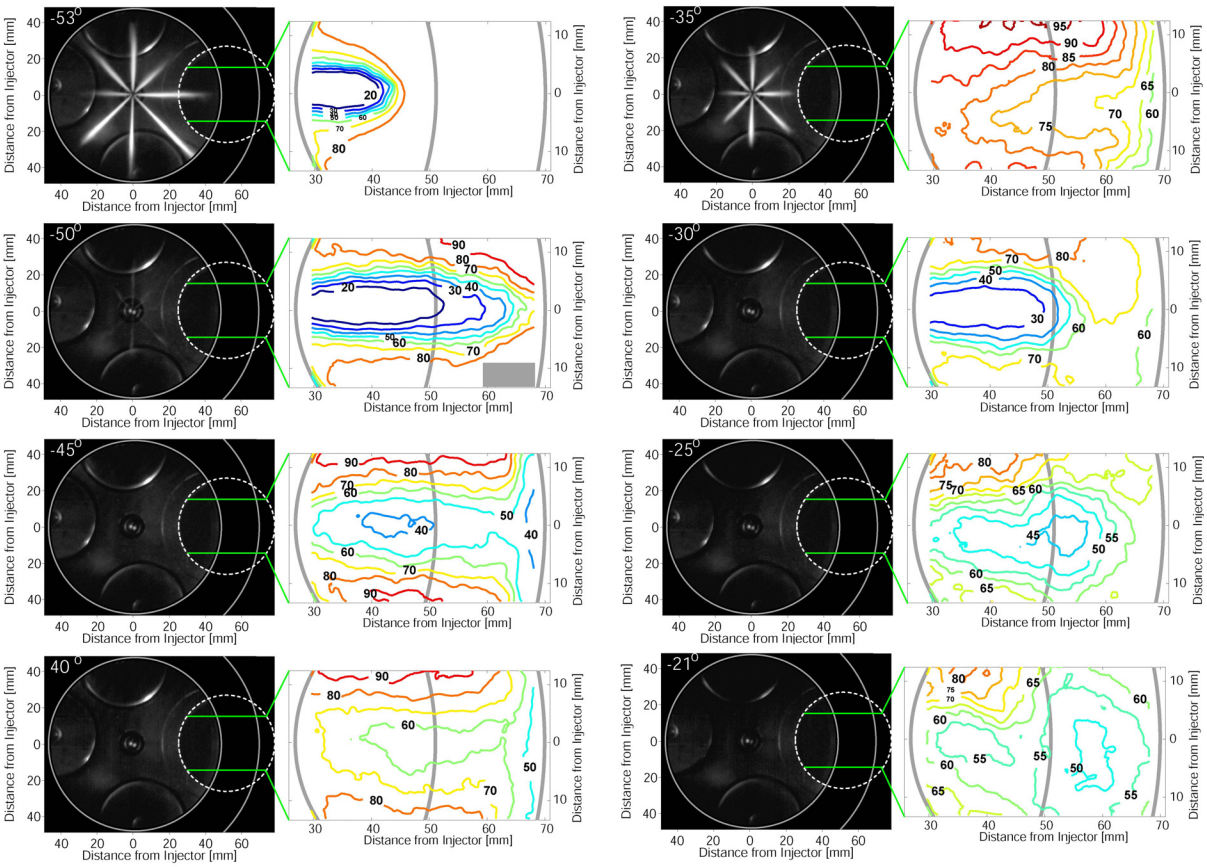

Figure 6. Sequence of liquid fuel HSC images (black background) and ensemble-averaged PRF maps at several times during the common-rail injection event. The time in crank angle degrees after TDC is shown in the upper left hand corner of each HSC image. The HSC images were acquired looking upward through the quartz piston bowl window and the PRF maps were generated from vapor fuel concentration measurements with the camera viewing downward through the cylinder head window. The FOV PRF maps is indicated by the dashed white line on HSC images. The location of the laser sheet is shown by the green lines. Note that the HSC images are from a single cycle and the PRF maps are derived from ensemble averaging 40 images.

second fuel injection, much of the fuel from the first common rail injection has mixed to create a relatively uniform mixture (on average) in the squish region around a PRF number of 70; however, in the upstream region, between the fuel jets, locations exists that are primarily iso-octane (on average). The final fuel-tracer PLIF image was recorded at -21° ATDC. At this time a small region in the downstream portion of the jet is at a PRF number near 50 and the PRF number increases on either side of the jet as well as upstream towards the injector.

Note that the optical access window in the cylinder liner becomes blocked by the piston bowl rim at crank angles later than -21° ATDC; therefore, no images are presented for later crank angles. Somewhat fortuitously, the low temperature heat release occurs around -20° ATDC; thus, the mixture distribution at -21° ATDC is likely representative of the distribution prior to fuel decomposition. Obviously further mixing will occur between -21° ATDC and ignition (around -7° ATDC); however, the fuel distributions prior to fuel decomposition are still useful to understand the observed combustion process.

The PRF maps show a broad distribution in fuel reactivity (i.e., PRF number) prior to ignition with a minimum PRF number around 50 in the center of the squish and a maximum PRF number around 80 in the upstream region between the fuel jets. The preferential downstream ignition observed in the chemiluminescence images appears to be the result of a region of high fuel reactivity (i.e., low PRF number) at the head of the jet created by the second common-rail injection event. The finding of a region of high fuel reactivity at the head of the jet is consistent with previous diesel-jet mixing measurements, which showed that after the end-of-injection, the fuel concentration increases with in-

creasing distance from the nozzle **[15]**. In the present study, the increase in fuel reactivity at the head of the jet created by the second common-rail injection is enhanced by the fact that much of the fuel from the first common-rail injection is located in the downstream region. Thus, as the jet mixes with the surrounding charge, the fuel reactivity in the upstream portion of the jet decreases further than that in the downstream portion of the jet.

After ignition, the chemiluminescence images show that the reaction zones tend to move from the outer region of the chamber to the inner region of the chamber until chemiluminescence is visible throughout the field of view (Figure 5). This finding is consistent with the observed fuel distribution prior to ignition. That is, regions of high fuel reactivity are found in the outer region of the chamber and the fuel reactivity decreases with decreasing axial distance from the injector. Note that, in the present study, fuel concentration measurements were only acquired in the field of view of the cylinder head window (see Figure 1); however, the results of the present study combined with previous work **[15]** suggest that the fuel reactivity will continue to decrease upstream toward the center of the chamber. It should also be noted that, while the chemiluminescence imaging is integrated along the (vertical) line-of-sight of the camera, the fuel concentration measurements show only a thin horizontal plane located 10 mm below the firedeck. However, given the abovementioned distribution in fuel reactivity, it can be inferred that the observed movement of the reaction zone from downstream to upstream is at least partially the result of the decreasing fuel reactivity from downstream to upstream. Also, from the present study it is not clear what role flame propagation plays on the reaction zone movement.

Conclusions

High-speed chemiluminescence imaging and toluene fuel tracer PLIF were used to investigate ignition and reaction zone progression for the dual-fuel RCCI combustion mode in a heavy-duty, optically accessibly research engine. RCCI operation was achieved by creating a well mixed charge of iso-octane using a GDI injector. Stratification in the fuel reactivity was introduced by a pair of common-rail injections of n-heptane.

The chemiluminescence imaging study showed that at the operating conditions explored in the present study, ignition generally occurred in the downstream portion of the jet – ignition sites were found both near the piston bowl rim and in the squish region. These ignition sites grew for several crank angle degrees and merged into larger reaction zones. In agreement with the chemiluminescence study, the fuel distribution showed that the region of highest fuel reactivity was located above the piston bowl rim. This region appears to be primarily the result of the second common rail injection; however, the increased reactivity in this region is enhanced by the already increased fuel reactivity due to the fuel from the first common-rail injection.

After ignition in the outer region of the combustion chamber, the reaction zone progressed inward toward the centrally mounted common-rail fuel injector. In agreement with the direction of reaction zone movement, the fuel tracer PLIF study showed that the fuel reactivity was the highest in the outer region of the combustion chamber and decreased with decreasing axial distance from the injector. Thus, it appears that the observed movement of the reaction zone is at least partially controlled by the gradient in fuel reactivity. The results of this study confirm that controlling the level of fuel reactivity stratification via dual-fuel operation is a promising method to control the rate of heat release for PCI combustion strategies.

Acknowledgements

The optical engine experiments were performed at the Combustion Research Facility, Sandia National Laboratories, Livermore, CA. Support for this research was provided by the U.S. Department of Energy, Office of Vehicle Technologies. Sandia is a multi-program laboratory operated by Sandia Corporation, a Lockheed Martin Company for the United States Department of Energy's National Nuclear Security Administration under contract DE-AC04-94AL85000. Financial support from the US Department of Energy (DOE) HCCI contract # DE-FC04-02AL67612 and from the Engine Research Center's Diesel Engine Research Consortium (DERC) member companies is gratefully acknowledged. The authors also express their gratitude to David Cicone of Sandia National Laboratories for his assistance with maintaining the optical-access research engine used in these experiments.

References

1. **Kokjohn, S. L., Splitter, D. A., Hanson, R. M., and Reitz, R. D.** Experiments and Modeling of Dual Fuel HCCI and PCCI Combustion using in-Cylinder Fuel Blending. *SAE International Journal of Engines*, 2010, **2**(2) 24-39.
2. **Hanson, R. M., Kokjohn, S. L., Splitter, D. A., and Reitz, R. D.** An Experimental Investigation of Fuel Reactivity Controlled PCCI Combustion in a Heavy-Duty Engine. *SAE International Journal of Engines*, 2010, **3**(1) 700-716.
3. **Splitter, D. A., Hanson, R. M., Kokjohn, S. L., and Reitz, R. D.** Reactivity Controlled Compression Ignition (RCCI) Engine Operation at Mid and High Loads with Conventional and Alternative Fuels. *SAE 2011-01-0363*, 2011.

4. **Sjoberg, M. and Dec, J. E.** Smoothing HCCI Heat-Release Rates using Partial Fuel Stratification with Two-Stage Ignition Fuels. *SAE 2006-01-0629*, 2006.
5. **Dec, J. E., Hwang, W., and Sjöberg, M.** An Investigation of Thermal Stratification in HCCI Engines using Chemiluminescence Imaging. *SAE 2006-01-1518*, 2006.
6. **Dec, J. E. and Hwang, W.** Characterizing the Development of Thermal Stratification in an HCCI Engine using Planar-Imaging Thermometry. *SAE International Journal of Engines*, 2009, **2**(1) 421-438.
7. **Kokjohn, S. L., Hanson, R. M., Splitter, D. A., and Reitz, R. D.** Fuel Reactivity Controlled Compression Ignition (RCCI) Combustion in Light- and Heavy-Duty Engines. *SAE 2011-01-0357*, 2011.
8. **Kokjohn, S. L., Hanson, R. M., Splitter, D. A., and Reitz, R. D.** Fuel Reactivity Controlled Compression Ignition (RCCI): A Pathway to Controlled High-Efficiency Clean Combustion. *International Journal of Engine Research*, (Accepted) 2010.
9. **Splitter, D. A., Hanson, R. M., Kokjohn, S. L., Rein, K., Sanders, S., and Reitz, R. D.** An Optical Investigation of Ignition Processes in Fuel Reactivity Controlled PCCI Combustion. *SAE International Journal of Engines*, 2010 **3**(1) 142-162.
10. **Genzale, C. L., Reitz, R. D., and Musculus, M. P. B.,** Optical Diagnostics and Multi-Dimensional Modeling of Spray Targeting Effects in Late-Injection Low-Temperature Diesel Combustion. *SAE International Journal of Engines*, 2009, **2**(2) 150-172.
11. **Splitter, D. A., Kokjohn, S. L., Hanson, R. M., and Reitz, R. D.** Injection Timing Effects in Dual-Fuel Premixed Combustion. *SAE 11ICE-0154*, (Submitted) 2011.
12. **Hultqvist, A., Christensen, M., Johansson, B., Franke, A., Richter, M., and Aldén, M.** A Study of the Homogeneous Charge Compression Ignition Combustion Process by Chemiluminescence Imaging. *SAE 1999-01-3680*, 1999.
13. **Genzale, C. L., Reitz, R. D., and Musculus, M. P. B.** Effects of Piston Bowl Geometry on Mixture Development and Late-Injection Low-Temperature Combustion in a Heavy-Duty Diesel Engine. *SAE International Journal of Engines*, 2008, **1**(1) 913-937.
14. **Hwang, W., Dec, J. E., and Sjöberg, M.** Fuel Stratification for Low-Load HCCI Combustion: Performance and Fuel-PLIF Measurements. *SAE Transactions*, 2007, **3**(116) 1437-1460.
15. **Musculus, M. P. B., Lachaux, T., Pickett, L. M., and Idicheria, C. A.** End-of-Injection Over-Mixing and Unburned Hydrocarbon Emissions in Low-Temperature-Combustion Diesel Engines. *SAE Transactions*, 2007, **116**(3) 515-541.
16. **Heywood, J. B.** Internal Combustion Engine Fundamentals. McGraw-Hill Inc., 1988, p. 508.
17. **Puduppakkam, K. V., Liang, L., Naik, C. V., Meeks, E., Kokjohn, S. L., and Reitz, R. D.** Use of Detailed Kinetics and Advanced Chemistry-Solution Techniques in CFD to Investigate Dual-Fuel Engine Concepts. *SAE 2011-01-0895*, 2011.
18. **Herold, R. E., Krasselt, J. M., Foster, D. E., Ghandhi, J. B., Reuss, D. L., and Najt, P. M.** Investigations into the Effects of Thermal and Compositional Stratification on HCCI Combustion - Part II: Optical Engine Results. *SAE 2009-01-1106*, 2009.
19. **Sjöberg, M. and Dec, J. E.** Effects of Engine Speed, Fueling Rate, and Combustion Phasing on the Thermal Stratification Required to Limit HCCI Knocking Intensity. *SAE 2005-01-2125*, 2005.